Computational and Experimental Evaluation of Nanoparticle Coupling†

Kevin L. Shuford,*,‡ Kent A. Meyer,‡ Cuncheng Li,§ Sung Oh Cho,§ William B. Whitten,‡ and Robert W. Shaw‡

Chemical Sciences Division, Oak Ridge National Laboratory, Oak Ridge, Tennessee 37831, and Department of Nuclear and Quantum Engineering, Korea Advanced Institute of Science and Technology, Daejeon, Korea, 305-701

Received: November 26, 2008; Revised Manuscript Received: January 5, 2009

We present theoretical and experimental studies on the optical properties of dimers composed of octahedron-shaped, gold nanoparticles. The experimental measurements show that the photoluminescence varies quite dramatically as two octahedra are brought into close proximity. AFM images and optical emission have been recorded for dimers in uncoupled and strongly coupled configurations. The former displays a single emission peak, while the latter shows two peaks with the new feature at longer wavelengths. Calculations indicate that the red-shifted peak originates from a strongly coupled plasmon state that oscillates along the extended axis of the dimer. Theoretically, we investigate the distances over which the dimers couple and find this to be particularly plasmon mode dependent. The anisotropic morphology and sharp apexes contribute significantly to the orientational dependence of the interparticle couplings and field properties.

Introduction

Noble metal nanoparticles support localized surface plasmon resonances in the visible wavelength regime that are strongly dependent upon many factors such as morphology, material, and local environment.[1−5] At resonant frequencies, the nanoparticle becomes highly polarized, and the oscillating charge emits an enhanced field. The extreme field amplification is ideal for many kinds of surface enhanced spectroscopies[6,7] and in some cases allows the detection of single molecules.[8−11]

When nanoparticles are close to each other, the excitations become coupled, and the optical properties can be vastly different from those of the isolated particle.[12−15] Here, we investigate both the weakly coupled and strongly coupled regimes using single particle microscopy and evaluate the strength of the nanoparticle coupling via shifts in the emission spectra. We are able to closely examine this coupling phenomenon using dimers composed of gold octahedra, which can be translated individually across a glass substrate. Our experimental setup allows for examination on a single nanoparticle basis and permits the manipulation of particles to form dimers—unique aspects of our effort. These experimental measurements are supported by classical electrodynamics calculations to elucidate the salient factors leading to strong interparticle coupling.

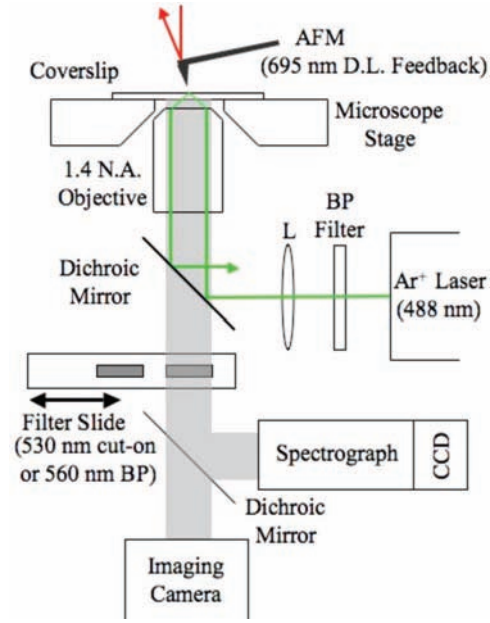

Figure 1. Schematic representation of the setup used for the experimental measurements.

Experimental Section

The octahedra investigated were synthesized using a modified polyol process[16,17] that yields single-crystal, gold nanoparticles with an octahedral shape. All of the measurements were of highly uniform octahedra with a 60 nm edge length dispersed on a glass coverslip.

Our correlated AFM-optical imaging instrument consists of a Veeco Metrology Bioscope AFM with the tip located directly above a Nikon Plan Apo 1.4 NA 60X oil-immersion objective used in a Nikon TE300 inverted microscope (Figure 1). The Bioscope AFM uses a diode laser (centered at 695 nm) to provide feedback for maintaining a constant height. The excitation source is a Coherent Sabre Ar^+ laser tuned to the 488 nm line. The laser light passes through a weakly focusing lens before entering the microscope yielding a laser power of approximately 5 mW. Upon entering the microscope, the light reflects off a Nikon B-2A dichroic filter and into the objective focusing to a spot size of ~25 μm. The lens, high numerical aperture objective, and translation of the laser beam toward the edge of the objective input aperture allow for a total internal reflection (TIR) geometry between a glass coverslip located at the ordinary focal point of the objective and the air above it.[18] Emission is collected back through the objective, dichroic, a

† Part of the "George C. Schatz Festschrift".

* Corresponding author. E-mail: shufordkl@ornl.gov.
‡ Oak Ridge National Laboratory.
§ Korea Advanced Institute of Science and Technology.

10.1021/jp810398s CCC: $40.75
Published on Web 02/11/2009

Schott glass OG530 cut-on filter (530 nm), and then passed to an imaging CCD (Princeton Instruments NTE/CCD-512-EBFT-GR-1) and to a spectrograph (Kaiser HoloSpec f/2.2 and PI Spec-10:400B CCD). The TIR geometry was employed to minimize scatter of the excitation laser off the reflective AFM tip.

Glass coverslips (FisherFinest #1) sparsely loaded with gold octahedra were generated by nebulizing a dilute methanol solution of the octahedra through a freshly tapered glass capillary using ultrapure nitrogen and then placing the coverslip in the spray path for several seconds.[19] The coverslips were baked in an oven at 90 °C for several hours and then inserted between the AFM and microscope objective for immediate use. Spectra were acquired with the AFM tip withdrawn (feedback diode laser off) and by aligning light from objects on the coverslip through the input slit of the spectrograph where an image plane was located. After 3−5 s of acquisition, the sample was translated (using a Prior Scientific H107N300 motorized stage) to a nearby area without nanoparticles, and a background spectrum was acquired for subtraction purposes. This two-step procedure was repeated for each object to avoid errors that might arise due to focal, scatter, and laser drift changes during the course of the experiment if we attempted to subtract a universal background file.

For nanomanipulation, the AFM diode laser was turned on and the tip re-engaged with the surface in a constant contact mode. A 50 nm bandpass interference filter centered at 560 nm was selected to eliminate the AFM diode laser light from entering the imaging CCD (see Figure 1). The tip coupled into the 488 nm TIR evanescent wave and resulted in an observable spot in the CCD image. The tip position was thus correlated with the optical image of the surface, and it was possible to observe the manipulation in real time. The stage was then moved via joystick control underneath the tip to assemble the octahedra into dimers. AFM imaging was performed by withdrawing and replacing the worn tip with a new one, re-engaging the surface in an intermittent ("tapping") mode, and realigning the tip with the nanoparticles. The imaging CCD was then turned off, and typical tapping mode AFM parameters were applied before scanning the object.

Results

We observed visually two distinct colors of photoluminescence for different particles. A series of AFM measurements indicated that small topographic features emitted green light, while the larger features emitted white light. We found this observation to correlate with emission from a single, 60 nm octahedron and clusters of octahedra, respectively. This rapid, visual method of discriminating between single nanoparticle emission and emission from aggregates (dimers, trimers, etc.) was used to search the slide for suitable structures to investigate.

Two green emission spots separated by >1 μm were identified, and AFM measurements confirmed that the individual surface features were indeed single octahedra. The tip was then used to carefully assemble the nanoparticles into a closely spaced dimer as shown in the AFM image (Figure 2). The diameter of the dimer is ∼165 nm, and the height is ∼50 nm, which are dimensions consistent with the size of two octahedra lying on triangular faces with a small interparticle spacing. We are unable to determine the exact spacing or orientation with our current experimental setup; however, we assume the spacing is a few nanometers. A plane of separation appears to run diagonally from the top left toward the bottom right of the figure, which may indicate a small spacing between octahedra. The phase

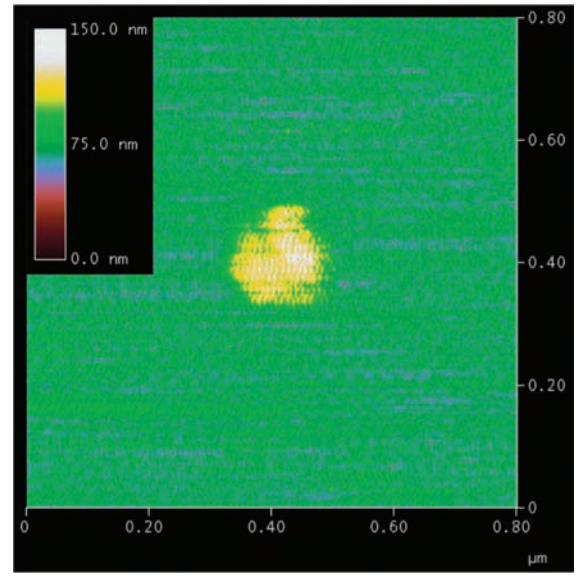

Figure 2. AFM image of a dimer composed of gold octahedra with 60 nm edges. The image indicates a 165 nm diameter and a 50 nm height, which are dimensions consistent with two closely spaced octahedra. Note that the substrate height is ∼70 nm on the color bar (i.e., the zero of the height scale has been shifted up 70 nm).

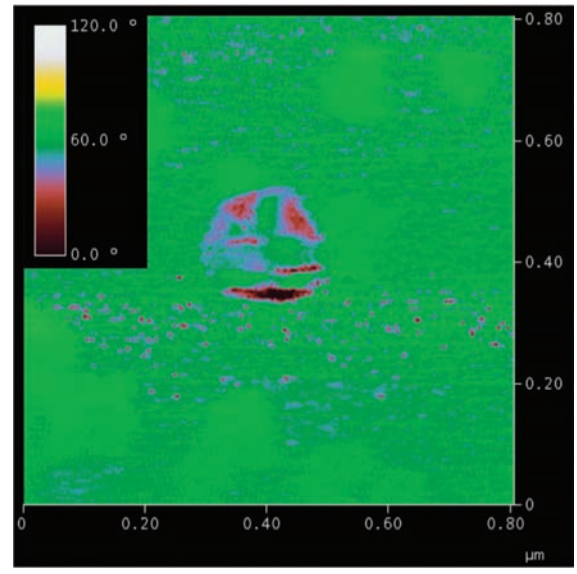

Figure 3. Phase representation of the octahedra dimer. The darker regions emphasize triangular faces.

image of the dimer is displayed in Figure 3. It is challenging to attach a physical meaning to the phase maps recorded under these conditions, yet we find that they often reveal a finer level of detail than AFM topographic information. For example, the darker regions appear to correspond to the triangular faces of an octahedron. We are confident that these images are indeed of a dimer and have created a movie showing the assembly of two octahedra in real time.

The photoluminescence from the dimers was recorded when the octahedra were spatially well separated and when they were closely spaced. Figure 4A displays a spectrum recorded when two octahedra were separated by large distances (>1 μm). Visually the emission appeared green indicating an uncoupled dimer configuration (essentially two individual nanoparticles). The emission was extremely bright, and a single emission peak centered at 560 nm was observed. We recorded the spectrum displayed in Figure 4B after assembling the same octahedra into

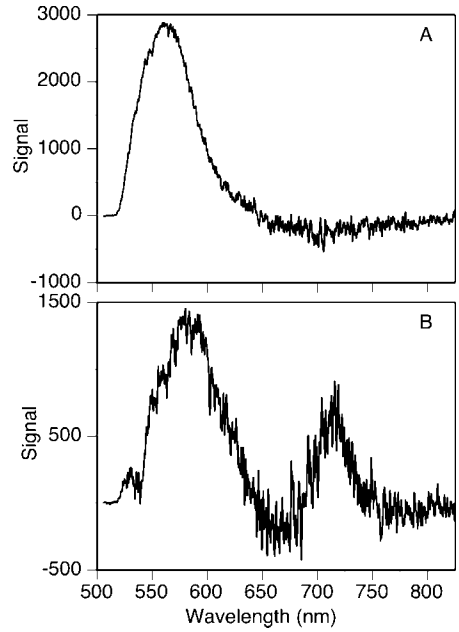

Figure 4. Measured emission from a dimer of 60 nm, gold octahedra. Panels A and B display the spectra recorded when the interparticle spacing was greater than 1 μm and a few nanometers, respectively.

a closely spaced dimer. This emission was generated by the dimer imaged in Figures 2 and 3. Note that the emission is distributed across the visible regime, which is consistent with the white color observed visually, and confirmed previously via AFM to be from closely spaced octahedra dimers. The emission spectrum consists of two peaks at 580 and 715 nm. The addition of a new spectral feature and the origin of its red shift are discussed in detail below.

Theory

The photoluminescence from gold nanoparticles has been shown to correlate well with nanoparticle extinction.[20,21] One mechanism proposed involves an interband excitation from d to sp states that decays nonradiatively into plasmon modes that then emit light. Both the width and location of emission bands have been shown to be consistent with the calculated extinction spectra of gold nanoparticles. Therefore, we will use calculated extinction spectra of gold, octahedra dimers to interpret our experimental photoluminescence data.

We have calculated the optical properties of gold octahedra using the Discrete Dipole Approximation,[22,23] which approximates the scattering volume by a square array of point dipoles. Each dipole obtains a polarization in response to the total field at that lattice site composed of the sum of an incident plane wave and the fields radiated from the other dipoles in the array. The value of the polarizability is obtained using a lattice dispersion relation[24] and incorporates the permittivity of the metal particle. We have chosen to use experimentally determined values for the permittivity of gold.[25] The resulting system of complex, linear equations is solved self-consistently for the polarization of each dipole. The extinction cross section is then calculated via the optical theorem from the induced polarizations and the incident field.

In the experiments, the octahedra reside on a glass coverslip. The calculations incorporate the surface effects in an average way by generating an effective dielectric function for gold. The effective permittivity contains components representing a particle completely embedded in vacuum and in glass. The coefficients scaling the components are based on the percentage of surface area in contact with each medium. Including the surface in this manner generates the correct global effects produced in the extinction spectrum but does not capture local interactions between the particle and surface.

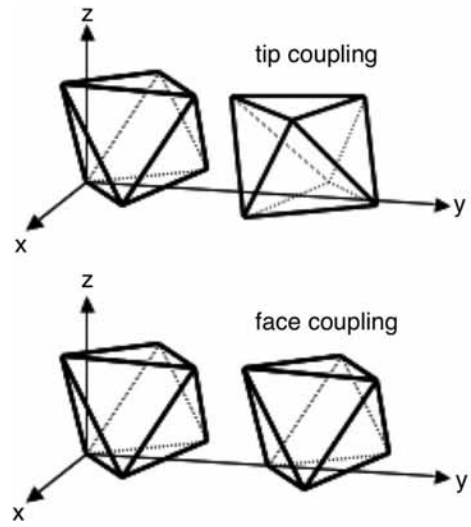

Figure 5. Schematic representation of the two coupling models used in the calculations.

Each nanoparticle is assumed to be a perfect octahedron with a 60 nm edge length and is oriented with one of the triangular faces on an imaginary surface ($x-y$ plane is the surface, apex of the triangular face at the origin, and the y axis bisects this face). Dimers are configured in two different arrangements as seen in Figure 5. Adding a second octahedron (in the $+y$ direction) as the mirror image of the first creates a tip-to-tip arrangement. That is, a reflection through an $x-z$ plane produces the second particle. The interparticle separation is defined as the tip-to-tip distance for this arrangement. A face-to-face arrangement is created by adding a second octahedron via a one-dimensional translation (along the $+y$ axis) of the first. Here the interparticle separation is defined as the distance between the two triangular faces. These two arrangements likely represent the extremes of interparticle coupling for octahedra dimers and should provide limits that other arrangements will fall between.

The optical properties of the anisotropic dimer are sensitive to the polarization of the incident field. We present results for two excitation conditions. If the incident field is polarized parallel to the major axis of the dimer, longitudinal plasmon modes will be excited. When the field is polarized perpendicular to the major axis of the dimer, transverse plasmon modes will be excited. Note that there are two transverse directions, but we find the results to be similar for both and only present the data for when the polarization is normal to the imaginary surface (z polarization) for clarity.

The calculated extinction spectra for gold, octahedra dimers are displayed in Figures 6 and 7 for tip and face coupling geometries, respectively. In both plots, Panel A shows the results for transverse modes, and Panel B displays the longitudinal modes. The trends in the optical spectra are similar for both the tip and face coupling models but are more pronounced for the latter. The transverse modes generate a slight blue shift and a decrease in peak intensity as the interparticle separation decreases from 100 to 3 nm. This implies a weaker coupling of the incident field to the dimer. The sum of absorption and scattering (i.e., the extinction) decreases, and the dimer becomes harder to polarize as is indicated by the blue shift. Conversely,

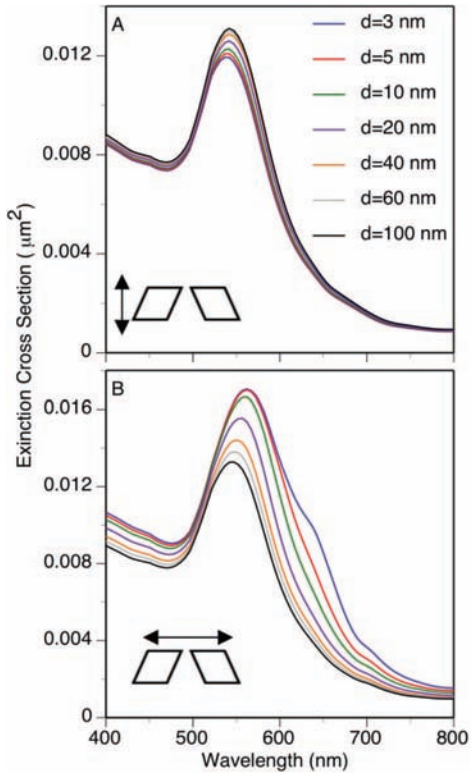

Figure 6. Calculated extinction spectra of dimers composed of 60 nm, gold octahedra in a tip coupling geometry. The traces indicate the tip-to-tip distance. Panels A and B show the transverse and longitudinal modes, respectively. The depiction in the lower left corner is a two-dimensional representation of the dimer and the polarization of the incident field.

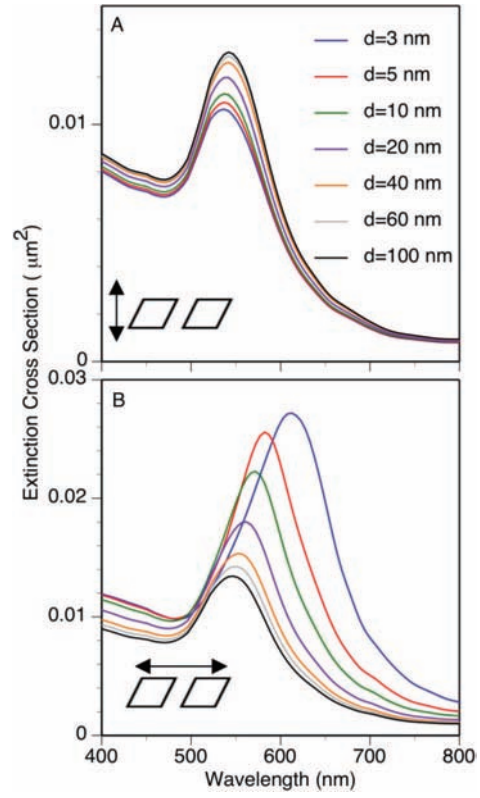

Figure 7. Calculated extinction spectra of dimers composed of 60 nm, gold octahedra in a face coupling geometry. The traces indicate the distance between triangular faces. Panels A and B show the transverse and longitudinal modes, respectively. The depiction in the lower left corner is a two-dimensional representation of the dimer and the polarization of the incident field.

the longitudinal modes red shift and increase in intensity as the particles are brought into close proximity. This suggests a strong interparticle coupling between octahedra, which are excited as a single entity via a resonant interaction with the incident field. The octahedra dimer is easier to polarize as is implied by the wavelength shift toward lower energies. These trends are reminiscent of what is observed in rods[2−4] and dimers composed of gold nanodiscs.[15]

Figures 8 and 9 more clearly display the shifts induced by interparticle coupling for the tip and face geometries. The shifts are calculated relative to the values at a separation distance of 100 nm, the same as a single particle, so the nanoparticles comprising the dimer are uncoupled at this distance. The tip coupling geometry does not yield any wavelength shifts until the particle separation is within an edge length (Figure 8A), yet the peak intensities do shift outside of that range (Figure 8B). For separations less than 60 nm, λ_{max} of the longitudinal modes shifts to longer wavelengths essentially linearly as the separation decreases. λ_{max} for the transverse modes is not affected until the particles are separated by less than 5 nm, at which point the excitation shifts to slightly shorter wavelengths. The magnitudes of wavelength and intensity shifts induced by longitudinal coupling are ~3 times larger than those of the transverse modes. Figure 9 shows the equivalent plot for the face coupling geometry. It is clear that the particles interact more strongly and over longer distances in this case. For example, the longitudinal dimer modes couple beyond 60 nm, and the red shifts induced scale exponentially with decreasing separation here. The transverse modes couple at distances less than 20 nm, which is four times that of the tip coupling result. In general, the transverse modes produce similar shift magnitudes for both coupling models, whereas the longitudinal modes

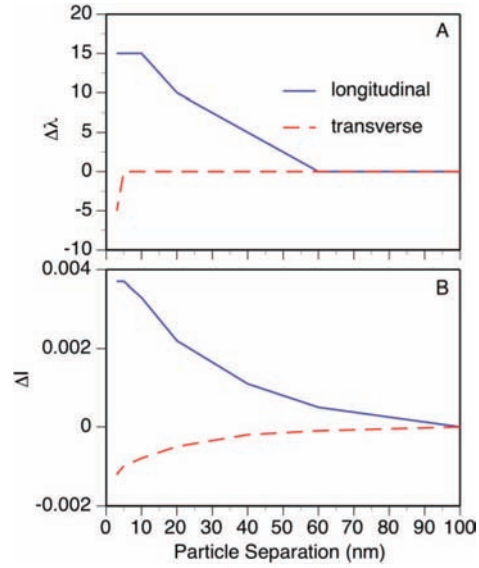

Figure 8. Shifts induced by tip coupling for the longitudinal and transverse modes. Panels A and B display the wavelength and intensity shifts, respectively. The shifts have been calculated with respect to the values at a 100 nm separation.

yield shifts for the face coupling scheme that are approximately four times that of the tip coupling scheme. This indicates that the nanoparticles are coupled most strongly in the face coupling geometry as is most conspicuous when exciting longitudinal plasmon modes.

From these observations, we can venture some general comments about upper bounds for representative coupling

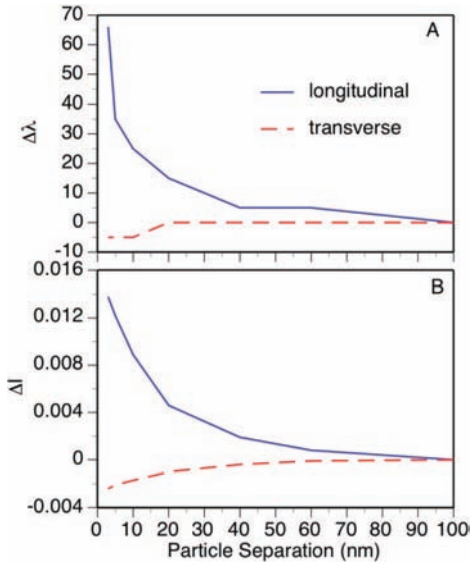

Figure 9. Shifts induced by face coupling for the longitudinal and transverse modes. Panels A and B display the wavelength and intensity shifts, respectively. The shifts have been calculated with respect to the values at a 100 separation.

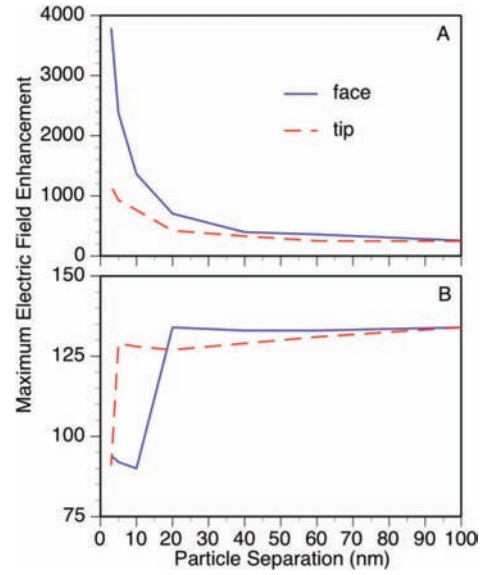

Figure 10. Maximum electric field enhancement for the face and tip coupling models. Panels A and B show the longitudinal and transverse excitations, respectively. Field enhancement is calculated relative to the intensity of the initial field.

distances in octahedra dimers. We find these distances to be mode (incident polarization) dependent as one might expect for anisotropic particles. The longitudinal modes couple over distances on the order of the edge length, with the face coupling scheme extending slightly beyond this. The transverse modes are weakly coupled until the interparticle separation is relatively small. This highlights the dependence of interparticle coupling on morphology, particle separation, and the plasmon modes generated since the magnitude of coupling varies significantly.

Discussion

At this point, we are able to discuss the comparison between theory and experiment. The experimental emission spectra (Figure 4) were recorded in a TIR geometry. The resulting excitation field is evanescent in nature and nominally unpolarized, so many different orientations are present for the measured signal. When the octahedra are well separated and uncoupled, a single peak is present as seen in Figure 4A. Calculations show that both the transverse and longitudinal plasmon modes reside at approximately the same wavelength when the dimer separation is 100 nm (the uncoupled regime), which is consistent with the single, more intense photoluminescence peak measured experimentally. A less intense, bimodal spectrum is produced when the octahedra are separated by a few nanometers and strongly coupled (Figure 4B). Calculations show that when the interparticle separation is small the longitudinal plasmon modes red shift significantly while the transverse plasmon modes are largely unaffected. We believe that the longer wavelength feature in Figure 4B ($\lambda = 715$ nm) results from strong coupling of the longitudinal modes, and the shorter wavelength feature ($\lambda = 580$ nm) is from transverse modes supported in the dimer. These findings are consistent with studies on coupled spherical nanoparticles under similar excitation conditions.[12,14]

The agreement between experiment and theory is reasonably good, but there are some discrepancies with regard to resonance wavelength. In general, the resonances predicted by theory are about the same width but blue-shifted from those measured experimentally. The uncoupled results measured experimentally (Figure 4A) and the calculations with 100 nm separations are within ~15 nm of each other. A filter function slightly distorts the spectrum observed experimentally, and the effect likely red shifts the recorded λ_{max} approximately 10 nm, which suggests better agreement with the calculations. Coupling the particles together experimentally (Figure 4B) produces two peaks that are red-shifted approximately 20 and 155 nm from the uncoupled peak. Theory predicts a very slight blue shift and a 65 nm red shift, respectively. While the magnitudes of the peak shifts do not agree quantitatively, the number of spectral features and relative coupling strengths predicted by theory are correct. Because we could not experimentally determine the orientation of the dimer components with great certainty, the calculations arbitrarily used two coupling motifs to investigate the system. It is probable that the large red shifts observed experimentally were generated by an orientation similar to the face-coupling model, as this arrangement generates the largest shifts. Moreover, the interparticle separation was never decreased to less than 3 nm in the calculations since a classical methodology was used here, and the validity of the results would be questionable. However, the trends in the calculations indicate that decreasing the interparticle separation to 1 nm would likely red shift the longitudinal plasmon mode to the region observed experimentally. It also worth noting other potential sources for the discrepancy between theory and experiment including different styles of excitation sources (evanescent wave versus plane wave), local surface contributions, inhomogeneity of the nanoparticle samples, and damage to the particles upon dimer assembly.

We have also calculated the electric fields around the dimers as the nanoparticles are brought into close proximity. The fields are dependent upon the exact particle morphology, and as with all grid-based methods, the values are sensitive to the size of the grid (~1 nm here). Figure 10 displays the maximum electric field enhancement as a function of interparticle separation for both the tip and face coupling geometries. The enhancement is defined as the intensity of the electric field ($|E|^2$) divided by the intensity of the incident field. At large separation distances, both coupling models converge to the same values indicating that particles are essentially uncoupled. The overall trends are similar to the extinction data in many ways. For example, the most significant enhancements with respect to interparticle separation

occur for longitudinal modes (Panel A), with the face coupled dimer generating the largest fields. The transverse modes display a decrease in the field magnitudes with decreasing separation, which is also reflected in the extinction data. It should be noted that the largest fields do not always reside between the two nanoparticles. In many cases, the maximum enhancements are found at apexes not directly composing a junction. This is especially true for the transverse modes, which only couple over shorter distances. The longitudinal modes more often display a junction effect, with the field maximum being between the overlapping regions comprising the coupled faces (note that these faces are rotated 60° from one another, Figure 5). The different field properties of the longitudinal and transverse modes reflect the need for adequate coupling to generate the junction effect, not merely closely spaced nanoparticles. Thoroughly understanding the field properties of noble metal dimers—as well as arrays—is important because they form the basis for many sensing platforms based on surface-enhanced Raman. Our results indicate that having closely spaced nanoparticles is not a sufficient condition to generate large field enhancements and that morphology and excitation conditions must also be considered, as they affect the extent of nanoparticle coupling.

Conclusions

We have investigated the effects of interparticle coupling on the photoluminescence from gold octahedra. An AFM tip was used to assemble two octahedron-shaped nanoparticles into a dimer structure. Far-field spectra were recorded in an uncoupled configuration (separation >1 μm) and in a strongly coupled configuration (separation $\sim$ a few nanometers). Weak coupling yields a single peak in the emission spectrum, and strong coupling produces two spectral features, one of which is significantly red-shifted. Calculations on octahedra dimers are in qualitative agreement with experiment and indicate that the longer wavelength feature results from a strongly coupled plasmon resonance oscillating along the extended dimer axis. Coupling distances in this orientation extend to greater than an octahedron edge length, while excitation with a perpendicular polarization produces coupling distances that are significantly shorter. The maximum electric field intensities follow trends similar to that of the extinction and show significant field enhancements localized between the nanoparticles when they are strongly coupled.

Acknowledgment. We are delighted to contribute to this issue honoring the life and work of George C. Schatz. One of us (K.L.S.) had the pleasure of working with George as a postdoctoral associate for three wonderful years at Northwestern University. This was a period of huge growth scientifically and personally for me, and I attribute this to the constant guidance and encouragement received. George's kind nature and towering intellect are a joy to all that know him.

This research was supported by the Division of Chemical Sciences, Biosciences, and Geosciences, Office of Basic Energy Sciences, U.S. Department of Energy under contract DE-AC05-00OR22725 with Oak Ridge National Laboratory, managed and operated by UT-Battelle, LLC. SOC was supported by a Korea Science and Engineering Foundation (KOSEF) grant funded by the Korean government (MOST).

References and Notes

(1) Millstone, J. E.; Park, S.; Shuford, K. L.; Qin, L.; Schatz, G. C.; Mirkin, C. A. *J. Am. Chem. Soc.* **2005**, *127*, 5312.
(2) Payne, E. K.; Shuford, K. L.; Park, S.; Schatz, G. C.; Mirkin, C. A. *J. Phys. Chem. B* **2006**, *110*, 2150.
(3) Kim, S.; Shuford, K. L.; Bok, H.-M.; Kim, S. K.; Park, S. *Nano. Lett.* **2008**, *8*, 800.
(4) Bok, H.-M.; Shuford, K. L.; Kim, S.; Kim, S. K.; Park, S. *Nano Lett.* **2008**, *8*, 2265.
(5) Shuford, K. L.; Lee, J.; Odom, T. W.; Schatz, G. C. *J. Phys. Chem. C* **2008**, *112*, 6662.
(6) Moskovits, M. *Rev. Mod. Phys.* **1985**, *57*, 783.
(7) Schatz, G. C. *Acc. Chem. Res.* **1984**, *17*, 370.
(8) Nie, S.; Emory, S. R. *Science* **1997**, *275*, 1102.
(9) Kneipp, K.; Wang, Y.; Kneipp, H.; Perelman, L. T.; Itzkan, I.; Dasari, R. R.; Feld, M. S. *Phys. Rev. Lett.* **1997**, *78*, 1667.
(10) Michaels, A. M.; Nirmal, M.; Brus, L. E. *J. Am. Chem. Soc.* **1999**, *121*, 9932.
(11) Xu, H.; Bjerneld, E. J.; Käll, M.; Börjesson, L. *Phys. Rev. Lett.* **1999**, *83*, 4357.
(12) Su, K.-H.; Wei, Q.-H.; Zhang, X. *Nano. Lett.* **2003**, *3*, 1087.
(13) Hao, E.; Schatz, G. C. *J. Chem. Phys.* **2004**, *120*, 357.
(14) Reinhard, B. M.; Siu, M.; Agarwal, H.; Alivisatos, A. P.; Liphardt, J. *Nano. Lett.* **2005**, *5*, 2246.
(15) Jain, K. J.; Huang, W.; El-Sayed, M. A. *Nano. Lett.* **2007**, *7*, 2080.
(16) Li, C.; Shuford, K. L.; Park, Q.-H.; Cai, W.; Li, Y.; Lee, E. J.; Cho, S. O. *Angew. Chem., Int. Ed.* **2007**, *46*, 3264.
(17) Li, C.; Shuford, K. L.; Chen, M.; Lee, E. J.; Cho, S. O. *ACS Nano* **2008**, *2*, 1760.
(18) Bartko, A. P.; Dickson, R. M. *J. Phys. Chem. B* **1999**, *103*, 11237.
(19) Lee, T.-H.; Kumar, P.; Mehta, A.; Xu, K.; Dickson, R. M.; Barnes, M. D. *Appl. Phys. Lett.* **2004**, *85*, 100.
(20) Hwang, Y.-N.; Jeong, D. H.; Shin, H. J.; Kim, D.; Jeoung, S. C.; Han, S. H.; Lee, J.-S.; Cho, G. *J. Phys. Chem. B* **2002**, *106*, 7581.
(21) Dulkeith, E.; Niedereichholz, T.; Klar, T. A.; Feldmann, J.; von Plesson, G.; Gittins, D. I.; Mayya, K. S.; Caruso, F. *Phys. Rev. B* **2004**, *70*, 205424.
(22) Draine, B. T. *Astrophys. J.* **1988**, *333*, 848.
(23) Draine, B. T.; Flatau, P. J. *J. Opt. Soc. Am. A* **1994**, *11*, 1491.
(24) Draine, B. T.; Goodman, J. *Astrophys. J.* **1993**, *405*, 685.
(25) Johnson, P. B.; Christry, R. W. *Phys. Rev. B* **1972**, *6*, 4370.

JP810398S